ARTICLE

Acoustofluidic Holography for Micro- to Nanoscale Particle Manipulation

Yuyang Gu, Chuyi Chen, Joseph Rufo, Chen Shen, Zeyu Wang, Po-Hsun Huang, Hai Fu, Peiran Zhang, Steven A Cummer, Zhenhua Tian, and Tony Jun Huang*

Read Online

ACCESS | Metrics & More | Article Recommendations | SI Supporting Information

ABSTRACT: Acoustic-based techniques can manipulate particles in a label-free, contact-free, and biocompatible manner. However, most previous work in acoustic manipulation has been constrained by axisymmetric patterns of pressure nodes and antinodes. Acoustic holography is an emerging technique that offers the potential to generate arbitrary pressure distributions which can be applied to particle manipulation with higher degrees of freedom. However, since current acoustic holography techniques rely on acoustic radiation forces, which decrease dramatically when the target particle size decreases, they have difficulty manipulating particles in the micro/nanoscale. Here, we introduce a holography technique that leverages both an arbitrary acoustic field and controllable fluid motion to offer an effective approach for manipulating micro/nano particles. Our approach, termed acoustofluidic holography (AFH), can manipulate a variety of materials, including cells, polymers, and metals, across sizes ranging from hundreds of micrometers to tens of nanometers.

KEYWORDS: acoustics, acoustofluidics, nanoparticle manipulation, cell pattern, acoustic tweezers
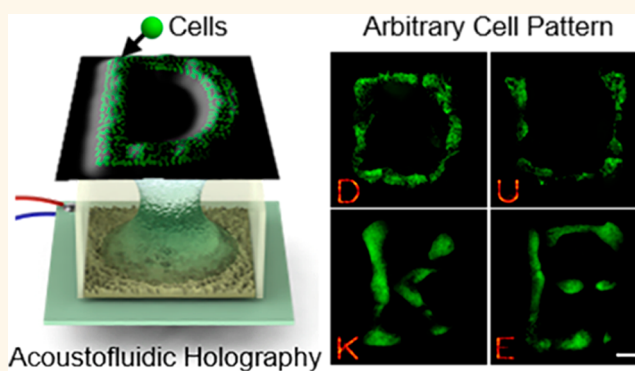
Over the past several decades, various techniques for manipulating particles have been developed, providing insights into areas such as protein folding[1] and enzyme kinetics.[2] These "tweezing" techniques, which include optical,[3] magnetic,[4] plasmonic,[5] and optoelectronic tweezers,[6] have been used to trap individual viruses, bacteria, and cells. Of these techniques, optical tweezers offer the highest degree of spatial resolution, and as a result they have been used in studies ranging from single molecule to cellular manipulation.[7] Although they are a powerful tool for force spectroscopy and biomolecular manipulation, optical tweezers require complex optics, including high-powered lasers and high numerical aperture objectives, and are potentially damaging to biological samples.[8] Acoustic-based particle manipulation techniques have emerged over the past decade as a noninvasive and label-free alternative to optical tweezers.[9−17] Although acoustic manipulation techniques may not offer the spatial resolution of optical tweezers, they possess advantages in terms of their ability to perform manipulations on a massively parallel scale and can control particles over a much larger size range from nanometers to millimeters.[18−20]

Several different platforms for acoustic-based particle manipulation have been successfully demonstrated. The most common design relies on the manipulation of standing wave fields.[11,21−24] In this approach, the interference between acoustic waves traveling in different directions generates a periodic, gridlike distribution of pressure nodes and antinodes, enabling particles of different properties to be trapped at specific positions.[25−29] Although simple to implement, these standing wave-based acoustic tweezers are constrained to particle trapping and manipulation in a gridlike spatial pattern. They are generally unable to form the customized, arbitrary patterns of particles needed for many applications in materials science, biology, and medicine. As an alternative to the common standing wave approaches, single acoustic beams (e.g., Bessel beams) have been utilized to trap individual particles in liquid,[30,31] similar to the configuration used by optical tweezers. With this method, single microparticles or droplets can be trapped and dynamically manipulated in three dimensions. Although this method enables the forces exerted
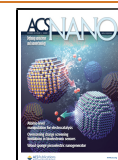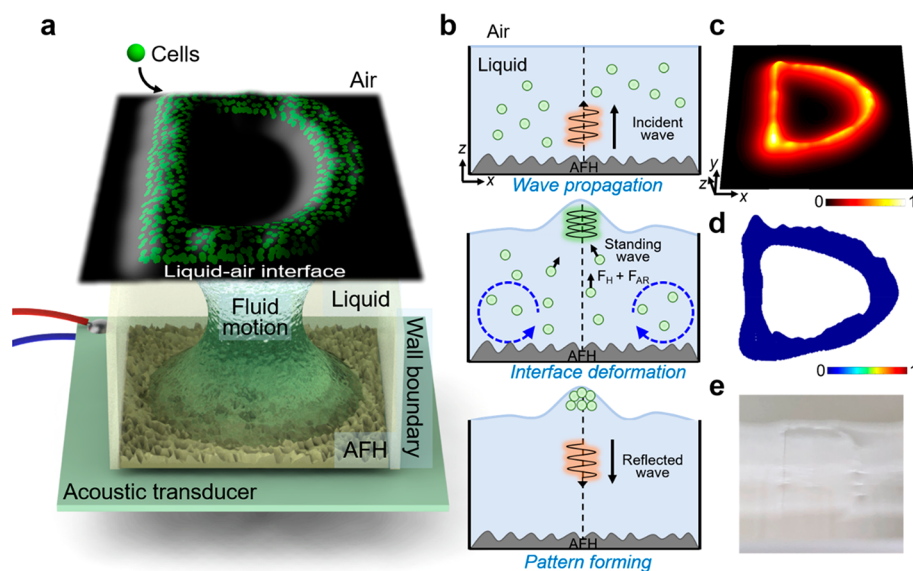
Figure 1. Schematic of the configuration and mechanism of cell/particle patterning via acoustofluidic holography. (a) Schematic of the experimental setup. The liquid−air interface serves as the image plane; cells/particles originally contained in the AFH structure are confined and translated to the designed pattern as acoustic waves are turned on. (b) Mechanism of acoustofluidic holography-based patterning. When the incident acoustic wave propagates to the liquid−air interface, the acoustic radiation pressure will deform the liquid surface. The resulting standing wave near the interface and the acoustic streaming bring the cells/particles to the wave crest and form complex patterns. F_H, hydrodynamic force; F_{AR}, acoustic radiation force. Blue circle: circulating streaming in the fluid domain confined by the boundary wall. (c) Designed interface deformation in the shape of the letter "D". (d) The pressure distribution of the deformed space. Because of the acoustic impedance mismatch, the pressure near the interface is zero. (e) Photograph showing the deformation when the acoustic wave is turned on.

on individual particles to be well controlled, with a single Bessel beam only one trapping position exists; this limits the use of single acoustic beams in high-throughput applications or biomedical applications where many cells or other bioparticles are often involved. Furthermore, unlike optical tweezers, which utilize a spatial light modulator to change the location of the trapping point, changing the focus of an acoustic beam requires a change in the position of the transducer or stage, leading to relatively large working areas and complex experimental setups.

Extensive research efforts have been made to achieve more complex pressure distributions through the use of acoustic metamaterials,[32] phononic crystals,[33,34] and phased arrays.[35] However, most research in these areas has been conducted using air as the transport medium, which restricts the use of these acoustic manipulation platforms; most biomedical applications require the manipulation of cells and bioparticles to be completed in their native liquid environment. Recently, acoustic holography, which was originally proposed for image reconstruction of physical objects,[36] has shown great potential for dynamic particle manipulation.[37,38] With regards to acoustic holography in the ultrasound regime, there are two commonly used configurations: either a phased array composed of multiple transducers is utilized,[35] or an acoustic kinoform is placed in the beam propagation path which discretizes and reconstructs the wavefront.[39] While results have been promising, the diffraction limit and fluid turbulence have limited current acoustic holographic technologies to manipulating relatively large (hundreds of micrometers), low-density particles which have negative acoustic contrast factors.[39,40] Similar trapping and manipulation using current acoustic holographic technologies have yet to be demonstrated for many particles of interest, including most cell types, extracellular vesicles, metals, and many polymers because most have positive acoustic contrast factors and are physically

smaller than 100 μm.[41] In general, most solid particles suspended in aqueous solutions have positive acoustic contrast factors,[41] meaning that current systems are severely limited in practical applications. Furthermore, these recent works ignore the fluid motion and induced hydrodynamic effect generated by the acoustic waves, which also contribute to particle movement.[42−45] Consequently, due to these constraints manipulation techniques based on acoustic holography have thus far been limited to niche applications and proof-of-concept demonstrations.

Here, we demonstrate an acoustofluidic holography (AFH) platform that overcomes the limitations of previous approaches and enables manipulation of micro/nanoparticles, such as cells, polymers, and metals, with a wide range of physical properties, in arbitrary spatial distributions and paths. Moreover, the combined acoustic and hydrodynamic physics employed in AFH enables the manipulation of particles with sizes as small as tens of nanometers, as well as the high-resolution patterning of individual cells. The experimental setup illustrated in Figure 1a is simple and versatile. The AFH platform is composed of an acoustic transducer and a 3D printed container with a custom-designed acoustic holographic kinoform at the bottom; the kinoform spatially modulates the phase of the incident acoustic plane wave from the transducer, and the container height is set to be the distance between the kinoform and the image plane. Diffraction of the incident wave creates a complicated but controlled three-dimensional pressure distribution pattern throughout the container where fluid is loaded to the same height as the container walls.

The AFH approach also involves a second component of particle manipulation in the form of engineered fluid motion. By controlling the acoustic radiation pressure and distribution, both inner and outer fluid deformation can be triggered as desired (i.e., liquid−air interface deformation and vortex
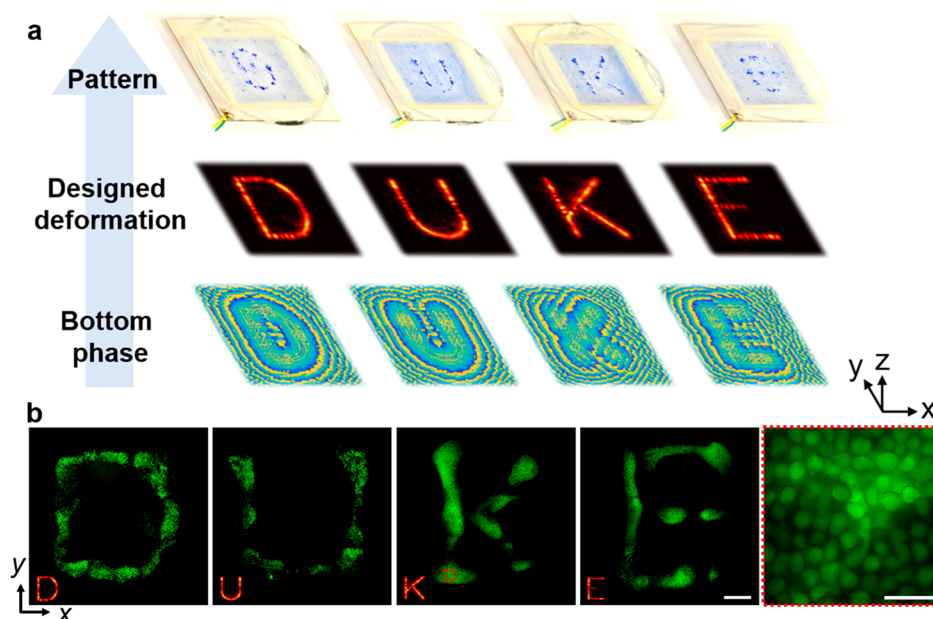
Figure 2. Cell and particle patterning via acoustofluidic holography. (a) The flowchart of the AFH-based particle/cell patterning process. The interface deformation patterns are designed and transferred to the corresponding pressure distribution, then back-propagated to derive the bottom phase distribution. When acoustic waves are turned on, blue 10 μm PS particles accumulate at convex surface deformation positions (top row showing photos of the patterns formed in the container). (b) Top-view (x−y plane) fluorescence images of patterned HeLa S3 cells and zoomed-in image of cells. Cell patterns of the letters: "D", "U", "K", and "E" are formed while the insets at the left corners show the calculated deformation pattern. Each patterned letter image is reconstructed from nine smaller fields-of-view captured by a microscope. Scale bar: 600 μm. (c) Zoomed-in image of patterned cells within the letter "K". Scale bar of zoomed-in image: 50 μm.

streaming). Thus, particles inside the fluid domain will experience both a hydrodynamic force and an acoustic radiation force. With acoustic waves propagating throughout the fluid, a circulating flow can be excited along the wave propagation path, while the side walls of the container can help to confine the fluid domain and minimize the evaporative driven fluid motion. This circulating flow provides the support to bring small particles to the liquid−air interface, which serves as the observing plane for the applications. Meanwhile, the acoustic radiation force simultaneously pushes the particles to specific position (e.g., forming nonaxisymmetric patterns or concentrating at a single spot). Different from previously proposed holographic-based manipulation techniques[39,40] which were implemented in an unbounded medium, here the AFH configuration has a finite size and the side walls of the container confine the fluid with nonslip boundary conditions. While it is shown to have very small impact on acoustic wave propagation (see Supporting Information (SI) Figure S1), the fluid motion inside the container can be better controlled and interact with the complex acoustic field. With the same experimental configuration, multiple functionalities are presented including patterning, rotation, concentration, and separation. Moreover, we show that by encoding dual patterns into one structure, different phenomena can be triggered under different excitation frequencies. This work presents an essential step for the use of holographic acoustic manipulation techniques in practical applications such as bioprinting, tissue engineering, cell separation, and micro/nanomaterial synthesis and assembly.

RESULTS AND DISCUSSION

As shown in Figure 1a,b, when an arbitrary engineered acoustic wave impinges on a liquid−air interface, the radiation pressure balances the gravity force acting on the fluid and generates a

steady deformation at this interface[46] (SI Figure S2). With this approach, the interference between the incident wave and the reflected wave generates a localized standing wave with the pressure nodes below the liquid−air interface (as shown in Figure 1b). Meanwhile, an acoustic streaming flow is generated toward the deformed space, which also corresponds to the lateral in-plane wave propagation direction (SI Figure S4b and SI Movie S1). Because of the combined effect of the acoustic radiation force generated by the localized standing wave and the hydrodynamic force generated by the in plane streaming, cells/particles migrate to the convex space and become trapped due to the balance of forces (see SI Figure S4 for the detailed patterning mechanism and SI Figure S5 for the typical measured pressure, streaming velocity, and force), thus forming the designed pattern (Figure 2 and SI Movie S2). The vertical deformation of the water surface h fits the pressure equilibrium equation

$$\rho_0 g h - \gamma \nabla^2 h = 2 p_r \tag{1}$$

where ρ_0 is the density of the water, g is the acceleration due to gravity, γ is the surface tension of the water, and p_r is the acoustic radiation pressure. The acoustic radiation can be indicated using the expression given by Gor'kov[47]

$$\boldsymbol{F}_{\text{rad}} = -\nabla \left\{ V_p \left[\frac{f_1}{2\rho_0 c_0^2} \langle p_1^2 \rangle - \frac{3\rho_0 f_2}{4} \langle \boldsymbol{v}_1 \cdot \boldsymbol{v}_1 \rangle \right] \right\} \tag{2}$$

where $f_1 = 1 - \frac{\rho_0 c_0^2}{\rho_p c_p^2}$, $f_2 = \frac{2(\rho_p - \rho_0)}{2\rho_p + \rho_0}$, V_p, ρ_p, c_p, ρ_0, and c_0 are the volume, density, acoustic velocity of the particle (with subscript of p), density, and acoustic velocity of the liquid (with subscript of 0), respectively. p_1 and v_1 are the pressure and velocity of the acoustic field.

Also, the hydrodynamic force resulting from acoustic streaming can be calculated with the measured flow velocity v[42]

$$F_H = 6\pi\eta a v \tag{3}$$

where η is the dynamic viscosity.

We first demonstrate patterning of 10 μm polystyrene particles as shown in Figure 2a. Then, we demonstrate cell patterning using HeLa S3 cells forming four letters: "'D'", "'U'", "'K'", and "'E'" at the liquid−air interface (Figure 2b). After the cells are transported to form the desired pattern, they subsequently will bond to each other and maintain their position and shape. Although the cell patterns may show some small gaps due to minor disruptions in the flow, the natural affinity of cells enable complex cellular arrangements to be fabricated via AFH. One interesting finding in the experiment is that the feature width of the actual cell pattern is observed to be smaller than the acoustic pressure field resolution ($\sim\lambda/2$). This improved patterning resolution is a result of the decreased width of the interface deformation pattern compared to the width of the pressure field (see SI Figure S6). Thus, as cells are trapped in the deformation space, they are confined in the area near the tip of the interface. To show the potential of AFH in more practical biological applications, we further demonstrated the use of AFH to pattern NIH3T3 cells in a Petri dish (SI Figures S9 and S10). Cells were placed in a hydrogel solution within the Petri dish, and the Petri dish was placed on top of the AFH device. Then, the cells were patterned by turning on the acoustic waves. The hydrogel was cross-linked subsequently by exposing to blue light to gelate the cell pattern in the hydrogel. Patterned cells were observed to grow and form clusters with the prescribed shapes.

Along with tissue level cell patterning, the ability to manipulate and pattern cells with high resolution offers many potential applications in the fields of biophysics, cell−cell communications, regenerative medicine, and tissue engineering.[35,37,39,40] With the common acoustic phase hologram, phase information covering from 0 to 2π is encoded in the bottom structure, which translates to numerous different thickness steps and requires high-resolution fabrication methods to fulfill the needs of high-frequency input. Here, we introduce the concept of binary phase AFH and show that it can be implemented to enable capabilities in high-resolution cell manipulation with commonly used rapid prototyping methods. In the binary AFH configuration, phase information is transferred from the transducer to the liquid domain using only two distinct "bits" in the kinoform design. These bits correspond to an acoustic phase of -0.02π or π rad, and represent theoretical 0's and 1's, respectively. With this binary phase AFH setup, although the mean square error will increase by roughly two times, corresponding to a lower fidelity, the phase steps required to generate the bottom kinoform are reduced significantly from thousands of distinct numbers to two values. The value of each binary pixel determines the thickness of the kinoform at that location, and variations in the thickness of the design that shift the phase by multiples of 2π will maintain the bit value. This means that larger height differences can be used to accommodate varying fabrication resolutions while achieving a high-resolution patterning capability for the binary AFH with higher frequencies. Thus, the required thickness resolution can be lowered to $\sim$30 μm compared to $\sim$0.1 μm for the common AFH design. As shown in Figure 3, 15 MHz is used to obtain a pixel width of 50 μm
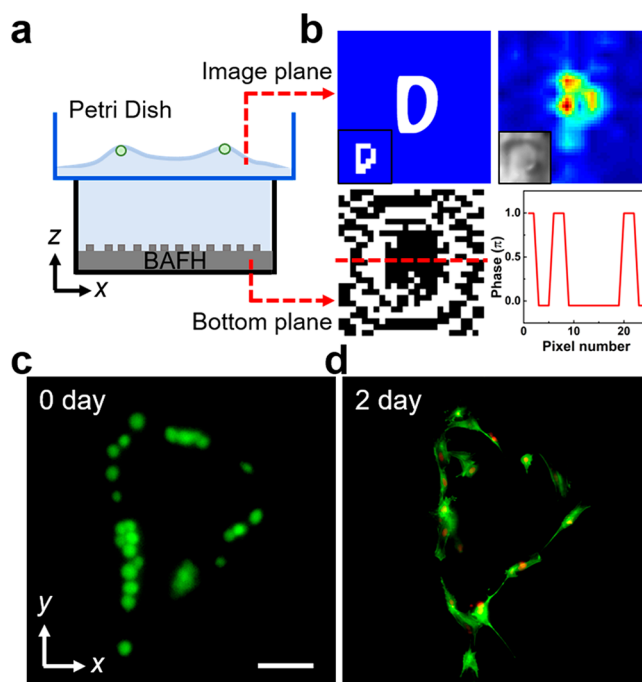

Figure 3. Binary acoustofluidic holography for high-resolution cell patterning. (a) Illustration of binary AFH-based high-resolution cell patterning. White area indicates "1" which corresponds to the phase of π rad, black area indicates "0" for -0.02 rad. (b) The original designed pattern with the letter "D", calculated pressure distribution, binary bottom phase, and phase distribution along the red dashed line. Inset: pixelwise designed pattern (left), microscopic image of the liquid−air interface (right). (c) Pattern of the NIH3T3 cells. (d) Cell growth after 2 days. Scale bar: 50 μm.

($\lambda/2$). While the pixelwise pressure distribution and interface deformation were designed as shown in Figure 3b, due to the acoustic radiation force in the interface deformation space and fluid streaming toward the deformation space, the actual pattern width is observed smaller than the pixel width (half of the wavelength), so that the pattern of the letter "D" is formed with high resolution. As a result, binary AFH can be used to form highly compact cell patterns and develop fibers with prescribed shapes after cultivation. It is also worth noting that high-frequency excitation may induce associated energy loss when combined with a 3D printed plastic structure due to the viscoelasticity and reflection by multiple interfaces (i.e., PZT to plastic and plastic to fluid). Thus, a trade-off between the desired frequency (e.g., 15 MHz), the spatial resolution, and the transmitted energy must be made when attempting to generate specific patterns.

In addition to the patterning of the particles inside the fluid domain, AFH is also able to drive single particle rotation in particles that are floating at the liquid−air interface. As shown in the Figure 4a,b, we designed a kinoform which can generate a vortex-shaped pressure distribution, corresponding to a circle-shaped interface deformation pattern with a concave position in the middle. Meanwhile, vortex streaming is generated in the bulk liquid near the interface, which can rotate the floating particle (SI Movie S3). With different excitation voltages, the streaming velocity and particle rotation speed can be controlled (see SI Figure S11b). The rotation speed is observed to be roughly proportional to the input power from 20 Vpp to about 45 Vpp, while beyond this point
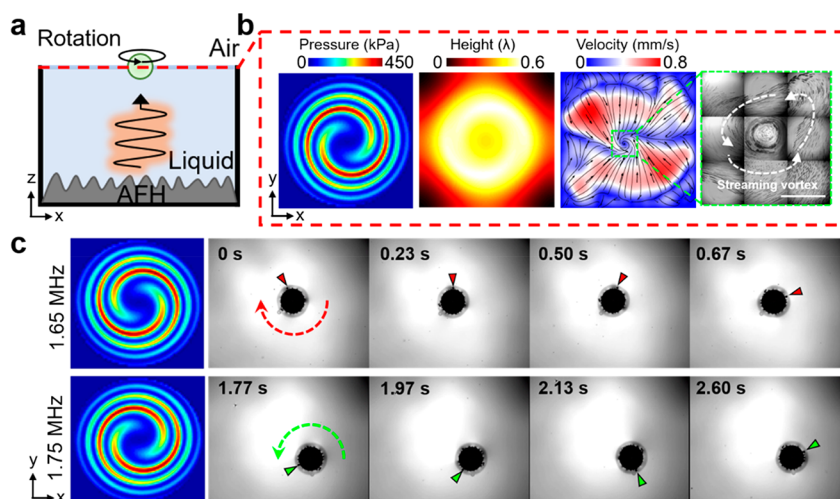
Figure 4. Single particle rotation via acoustofluidic holography. (a) Illustration of AFH-based rotation. A hydrophobic particle which remains floating on the liquid−air interface was used here. Inset **(b)** shows the pressure field, interface deformation, and calculated and experimentally observed flow fields. Scale bars: 50 μm. **(c)** Two different pressure fields are encoded into one AFH structure for reversible rotation. When excited at 1.65 MHz, the particle will rotate clockwise along with the vortex streaming. When switched to 1.75 MHz, the rotation direction is reversed due to the pressure field change. Scale bars: 250 μm.

the precession of the particle inhibits further improvements of the rotation speed.[30] Moreover, two distinct pressure distributions can both be encoded into a single AFH structure with different frequencies exciting the differing patterns,[48] which enables us to tune not only the speed of the particl but the direction of rotation as well. As shown in Figure 4c, two vortex-shaped pressure distributions with counterclockwise and clockwise polarities are encoded with excitation frequencies of 1.65 and 1.75 MHz, respectively. Under 1.65 MHz excitation, the acoustic pressure distribution generated is a counterclockwise vortex, resulting in clockwise rotation of the particle. As the frequency is switched to 1.75 MHz, the particle will rotate in the clockwise direction due to the altered acoustic pressure and streaming fields (SI Movie S4).

We further demonstrate the manipulation of different types of particles and cells by the acoustic vortex in which the appropriate amplitude and phase information is simultaneously encoded into a single structure (Figure 5a,b and SI Movie S5). While the most commonly used acoustic holography methods modulate the acoustic pressure or phase independently, here we utilize double-phase holography to enable full wave modulation that can generate a more complex acoustic field using a single, low-cost structure. In our study, by decomposing the complex acoustic field into two phase components, an acoustic vortex with a spiral-shaped phase distribution as well as a vortex-shaped pressure field is designed. With this configuration, a 3D vortex streaming field is observed in the bulk liquid with both horizontal and vertical streaming (see SI Figure S12). As the vertical circulating flow is generated akin to the Eckart streaming, angular momentum can be transferred to the fluid due to vortex phase. Similar to the previous cell pattern phenomenon, with the image plane set in the near field particles are observed to form the vortex-shaped pattern. But interestingly, by increasing the distance between the bottom structure and image plane (∼40 λ), we found that instead of forming the vortex-shaped pattern, particles tend to migrate to the middle of the liquid−air interface. This phenomenon may be due to the increased attenuation of the acoustic wave at longer propagation distances and subsequent transfer of energy and
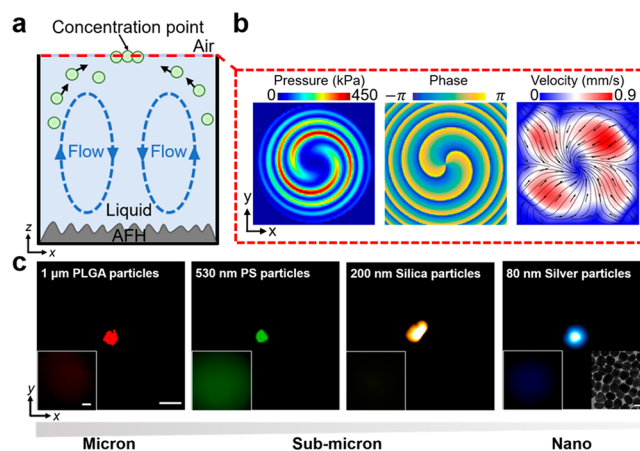

Figure 5. Particle/cell concentration via acoustofluidic holography. (a) Illustration of the particle/cell concentration mechanism detailing the process of AFH-induced vortex streaming in both horizontal and vertical directions. Particles are ultimately concentrated at the center of the AFH device, along the liquid−air interface. **(b)** The pressure distribution, phase, and flow field of the designed image plane. **(c)** Particles with different physical properties and sizes ranging from micrometers to nanometers can be concentrated via AFH. Insets: initial states of the particles before the acoustic signal is turned on (left), TEM image of the extracted silver nanoparticles (right). Scale bars: 100 μm for fluorescent images and 100 nm for TEM image.

angular momentum to the surrounding fluid. Thus, we further investigated how the vertical and lateral hydrodynamic forces and acoustic radiation force influence the pattern with different distances between the bottom of the devices and the image plane. As shown in SI Figure S13c,d, we found that with relatively small distances (∼10 λ), particles tend to form the vortex-shaped pattern, while with larger distances (∼40 λ) particles are concentrated and form the disklike pattern. We theorize that the reason for this observation is that with smaller distances, acoustic waves are less attenuated and the acoustic radiation force plays a more important role in forming the pattern; with larger distance, as we discussed above, acoustic
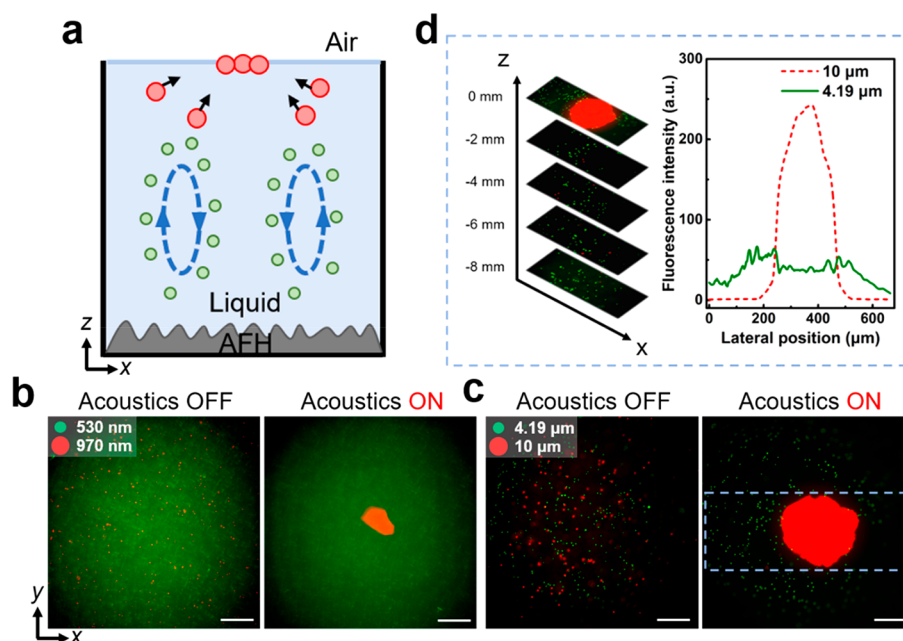
Figure 6. Particle/cell separation via acoustofluidic holography. (a) Illustration of the selective concentration mechanism. Larger particles will experience a larger acoustic radiation force and hydrodynamic force which enables them to be separated from the mixture solution. (b) Separation of 970 and 530 nm particles. Scale bar: 100 μm. (c) Separation of 4.19 and 10 μm particles. Scale bar: 200 μm. (d) Fluorescent images at different z-planes and fluorescent intensity distribution along the lateral axis.

waves have larger attenuation along the z-axis, and particles are brought to the middle of the interface by the acoustic streaming. This results in increased vertical streaming and enables small particles to be concentrated along the streamline to a single spot near the liquid−air interface (Figure 5). The acoustic waves in this configuration simulate a stick stirring the liquid, thus, in order to maintain the curved path of the liquid motion, a centripetal force is needed to direct particles toward the center. Meanwhile, the acoustic radiation force will continuously help to trap the particles near the interface.

Utilizing both the acoustic radiation force and hydrodynamic force in the bulk liquid, we are able to concentrate particles and form a disk-shaped pattern with particles that have different material properties and sizes ranging from tens of micrometers to tens of nanometers (as shown in Figure 5c and SI Figure S13, SI Movie S6), as well as for living matter (E. coli bacteria) which has a self-propulsive force. With an excitation frequency below 10 MHz, the acoustic radiation force and hydrodynamic force balance each other and create a size limit of ~1 μm; however, the motion of submicron and nanosized particles is dominated by hydrodynamic force. With a weak acoustic radiation force and vertical hydrodynamic force, particles are brought to the interface and then follow the streamlines (see SI Figure S12) to be gradually concentrated at the middle of the interface.

In addition to concentrating the particles/cells for applications such as biosensing, cells can also be patterned into disklike shapes and further connect with each other after culture (SI Figure S14). This function may be beneficial in biomedical applications[49] such as tumor modeling and cancer therapy. In the experiments, 1.65 MHz acoustic waves are used to concentrate the particles larger than 1 μm while 7.21 MHz waves are used to concentrate the submicron and nanoparticles. Cell viability testing was also performed to study the influence of the acoustic wave and hydrodynamic effects. Both the concentrated and control cells tested are shown in SI

Figure S15. The results show over 95% viability in the concentrated sample, suggesting that AFH is a highly biocompatible manipulation technique.

Matching theory with experimental results, we found that the concentration phenomenon corresponds to the relationship between the excitation frequency, amplitude, and particle size. When the liquid contains a mixture of particles with different sizes, larger particles move along the vertical circulating streaming and reach the interface faster due to relatively larger acoustic radiation force and are also pushed toward the middle due to the lateral hydrodynamic force. Meanwhile, the smaller particles follow the circulating streaming direction and are brought back to the fluid domain by the hydrodynamic force, preventing their vertical migration. These differences in particle trajectories allow us to separate particles with different sizes (SI Movie S7). As shown in Figure 6 and SI Figure S16, by using different combinations of frequency and power, we can separate 970 nm particles from 530 nm particles, 1 μm particles from 3 μm particles, and 4.19 μm particles from 10 μm particles. We observe that the fluorescent intensity in the middle area of the surface is significantly larger than the surrounding area, which indicates that the majority of the 10 μm particles have migrated to the center. On the other hand, the 4.19 μm particles remain randomly distributed since the acoustic radiation force and lateral hydrodynamic force they experience is not comparable to the vertical hydrodynamic force. The significant contrast in the concentration density of particles with different sizes demonstrates the potential for using AFH for particle separation based on differences in size.

CONCLUSIONS

In this study, we introduce a multifunctional acoustofluidic holography technology. Contrary to conventional acoustic-based particle manipulation, which requires standing wave fields with gridlike pressure node distributions or complex

configurations to trap particles, the AFH device described here confines the complex acoustic wave distribution and fluid to a small space where acoustic streaming can be harnessed to stimulate fluid motion and further manipulate particles in either translational or rotational manners. A combination of acoustic radiation forces and hydrodynamic forces can manipulate particles with different material properties and sizes, enabling many potential applications in various fields. Meanwhile, with the same experimental configurations different holography techniques are explored in our studies to achieve different types of engineered fluid motion. These techniques include the classic phase holography, which is used to generate a predesigned pressure or phase distribution, as well as multiple-frequency holography, which is used to generate distinct acoustic fields under different excitation frequencies. In addition, double-phase holography is introduced to simultaneously modulate the pressure and phase fields, which brings a higher degree of freedom during particle manipulation.[50] Finally, binary holography is utilized to achieve high-resolution cell patterning. Techniques for high-resolution cell patterning typically require the use of complex equipment or expensive fabrication techniques; however, binary holography enables high-resolution cell patterning using an easily accessible, low-cost fabrication technique (i.e., 3D printing). While various binary holography studies have been conducted in optics,[51,52] it has been previously unexplored in the field of acoustic manipulation. One potential reason for this discrepancy is because in optics an amplitude binarized field can be relatively easily achieved via a photomask or spatial light modulator; however, acoustics faces technical challenges due to its strong transmission effect in liquid, which leads to difficulties in fabricating a binary amplitude kinoform for underwater acoustics. In our study, we applied a binary phase holography method which avoids the amplitude modulation and simplifies the fabrication criteria, thus, shortening the bridge between high-resolution particle patterning and low-cost devices.

In addition to the holographic modulation of the acoustic wave, the resulting engineered fluid motion (i.e., liquid−air interface deformation and acoustic streaming) is equally important to the performance of AFH. For example, we have demonstrated that liquid−air interface deformation is essential for cell patterning; when a thin coverslip is placed on top of the liquid surface to prevent the interface deformation, cells can no longer be patterned and instead remain suspended in the fluid domain (see SI Figure S7). Liquid−air interface deformation is required for cell patterning because it provides a stable space where cells can be trapped. In addition, the interface serves as a natural barrier that prevents the vertical migration of cells away from the patterned area due to undesired turbulent flow. As a result, the actual cell pattern formed near the interface shows a narrower feature width than the designed acoustic pattern due to the decreased width of the deformation space, leading to a "resolution breakthrough" phenomenon as compared to the acoustic field resolution alone. The interface deformation interaction can also be seen as a type of low-pass filter[53] that is able to remove noise from the acoustic field pattern, which without filtering typically exhibits roughness in its 2D projection (see SI Figure S8). As such, cell patterns formed in the deformation space are clearer compared to the patterns dominated by purely acoustic radiation forces. Noting that although a recently reported soft membrane-based acoustic particle patterning method can also achieve complex and

nonperiodic cell patterning with a thin PDMS structure,[54] their method still heavily relies on complex fabrication techniques and acoustic radiation force-based manipulation. In addition, the target sample volumes (a thin liquid layer) are limited by the fragile thin film structure. Compared to their design, our AFH technology has advantages in its ability to not only pattern particles, but also rotate, concentrate, and separate particles. As a result, AFH can be more easily implemented as a robust experimental platform.

In summary, we demonstrate four different functionalities using acoustofluidic holography including: patterning, rotation, concentration, and separation using either biological samples or micro/nanoparticles (see SI Figure S17 for the design flowchart for different functions). Although only four basic functions are shown here, more complex functions and applications (e.g., size-selective cell patterning and enrichment, nanocapsule synthesis) can be envisioned based on this versatile platform. Furthermore, the working sample volume can be conveniently adjusted (from ∼10 μL to ∼1 L) depending on the required application. With the binarized kinoform developed in this work, not only is the design of the device simplified, but the subwavelength structured kinoform can be fit to higher excitation frequencies which enables the manipulation of cells into prescribed patterns with high resolution. With higher-resolution fabrication techniques (e.g., nanofabrication), the patterning resolution can be further enhanced. Encoding several acoustic pressure designs or prescribed amplitude-phase distributions into one structure allows different functions to be performed simultaneously or individually with a single device. Although our AFH contains a relatively small number of pixels (from ∼600 to ∼9000 pixels, 1 pixel is a square with the length of half of the wavelength) compared to previous work (∼15 000 pixels),[39] it is enough to drive fluid motion and allows for fluid control and particle manipulation; the AFH design strategy can also be extended to larger scales with more pixels and larger volumes. Ultimately, this AFH technology greatly simplifies the experimental setup of current acoustic-based particle manipulation techniques while achieving the high spatial resolution and versatility required for a diverse set of applications in materials science, biology, and medicine.

MATERIALS AND METHODS

Design of the Acoustofluidic Holographic Kinoform. The iterative angular spectrum method[36,55−57] is applied here, where the surface deformation computation can be calculated by combining the intensity distribution with a transfer function derived from the pressure equilibrium equation.[53] The surface deformation can be indicated as

$$H_s(k_x, k_y; z_s) = P_r(k_x, k_y; z_s)G(k_x, k_y; z_s) \tag{4}$$

where k, k_x, k_y indicate the wavenumber in join, x, y directions, respectively, z_s, z_b are the vertical coordinates of the liquid surface plane and bottom plane, respectively. The calculated transfer function $G(k_x, k_y; z_s)$ is

$$G(k_x, k_y; z_s) = \frac{1}{\rho_0 g + \gamma(k_x^2 + k_y^2)} \tag{5}$$

where ρ_0 is the density of the liquid, g is the gravity acceleration, and γ is the surface tension of the liquid. $P_r(k_x, k_y; z_s)$ is the Fourier transform of the acoustic radiation pressure which is expressed as

$$P_r(k_x, k_y; z_s) = \mathcal{F}\left(\frac{p(x, y; z_s)^2}{\rho_0 c_0^2}\right) \tag{6}$$

where $p(x,y;z_s)$ is the pressure distribution on the z_s plane.

On the basis of the angular spectrum method, we have

$$P(k_x, k_y; z_s) = P(k_x, k_y; z_b)e^{j(z_s-z_b)\sqrt{k^2-k_x^2-k_y^2}} \tag{7}$$

This allows us to relate the bottom pressure to the interface deformation through the following relationship

$$\mathcal{F}\left\{\sqrt{\mathcal{F}^{-1}\left[\frac{H_s(k_x, k_y; z_s)}{G(k_x, k_y; z_s)}\right]\rho c^2}\right\}$$

$$= P(k_x, k_y; z_s) = P(k_x, k_y; z_b)e^{j(z_s-z_b)\sqrt{k^2-k_x^2-k_y^2}} \tag{8}$$

Thus, by designing for the desired deformation at the liquid−air interface, we can back calculate the pressure distribution to the image plane. Further back-propagation allows us to predict the phase distribution of the bottom plane and design the required 3D printed kinoform structure. The derivation is detailed in the Supporting Information.

When designing the acoustofluidic holography device, we first decompose the input from the bottom pressure field into multiple spatial frequency components by a 2D Fourier Transform and propagate to the interface. Then, multiple transfer functions are used to calculate the surface deformation. The deformation amplitude for the interface can be converted to the pressure distribution at the interface. After that, the pressure distribution along the bottom can be obtained, enabling us to calculate the required thickness of the 3D printed kinoform structure at each spatial location. Several iterative processes need to be employed in order to minimize the erroneous components.

It is worth mentioning that as $\sqrt{k_x^2 + k_y^2}$ approaches k, the spectral transfer function $h(k_x, k_y; z) = e^{j(z_s-z_b)\sqrt{k^2-k_x^2-k_y^2}}$ is inherently undersampled in this region which causes aliasing errors. To address this problem, we applied spatial frequency truncation and the cutoff spatial frequency is given by[58]

$$k_{cut-off} = k\sqrt{\frac{D^2}{D^2 + 2(z_s - z_b)^2}} \tag{9}$$

where D is the length of the bottom structure. This cutoff eliminates the under sampled angular spectra and protects the imaging plane from the influence of higher spatial frequency components.

Design of Acoustic Vortex Shapes. The process to design the acoustic field to generate the 2D vortex shape is similar to the design process for shaping the deformation of the liquid−air interface. We utilize a band limited iterative angular spectrum method which leads to 2D vortex streaming with a propagating acoustic energy flux. The amplitude is controlled during the calculation and back-propagated to form the phase map. Since the particle is floating on the liquid−air interface, only 2D vortex streaming is utilized here and the vertical streaming in the fluid domain will not influence the rotation performance.

The design of the 3D acoustic vortex field with 3D streaming is obtained with the help of double-phase holography, which transfers the amplitude and phase separately (details in Supporting Information). With the image plane setting on the liquid−air interface, a 2D vortex streaming similar to the particle rotation case is generated. Meanwhile, there are two vortices streaming in the vertical direction which also contribute to the motion of the particles immersed in the liquid. Instead of generating an exact vortex pressure distribution in a free field, the acoustic field is used to initiate the vortex and transfer angular momentum near the interface when the body force is perpendicular to the interface. As for the 3D vortex streaming design, particles are pushed to a single point in the fluid

domain with a relatively large volume, which is difficult to achieve using traditional acoustic tweezers.

Meanwhile, in the near-field holographic calculation, the higher spatial frequency components have very little influence on the field distribution. This is because most of the higher spatial frequency components are directed toward the middle area of the surface. Thus, even in free space the forward propagating wave will mostly travel toward the surface instead of being reflected by the wall. In addition, the wall is designed to be thick enough to dissipate most of the energy of the components with higher spatial components. Therefore, even though the wall and water have similar acoustic impedances, the wall has a much higher attenuation as compared to the water. The detailed discussion comparing the free-space propagation and confined space propagation is presented in the Supporting Information.

Dual-Frequency Acoustofluidic Holography Design. Reversible clockwise and counterclockwise particle rotation is achieved by encoding two vortex shape distributions into one structure. This exploits the chromatic variation within the Fresnel focal depth for multiple frequencies. When two different pressure distributions are encoded into one structure, both of the fields exist simultaneously once the transducer is turned on with either designed frequency applied.[48,59] The pressure field will be in-plane with one corresponding excitation frequency while the field respective to the other frequency will be out-of-plane due to the wavelength dependence of the phase offsets during propagation. The relationship between the two frequencies and two imaging distances is approximated as

$$f_{ac} d_{ac} = f_c d_c \tag{10}$$

where f_{ac}, f_c, d_{ac}, and d_c are the frequency designed for a counterclockwise vortex, the frequency designed for a clockwise vortex, the imaging distance of the counterclockwise vortex, and the imaging distance of the clockwise vortex, respectively.

As the phase offset generated by the structure is calculated, the thickness map of the structure can be described by

$$t(x, y) = t_o - \frac{\Delta\varphi(x, y)}{k_s - k_l} \tag{11}$$

where t_o is the original settled thickness, $\Delta\varphi(x,y)$ is the calculated phase map, k_s is the wavenumber of the structure, and k_l is the wavenumber of the liquid. Then, the thickness map is converted to the real structure using a 3D printer (MJP3600, 3D Systems, U.S.A.) with a crystal material whose acoustic velocity and density are measured as 2350 ± 50 m/s and 1.22 g/cm^3, respectively. The printer's spatial resolution limit is x,y, 33 μm; z, 13 μm.

Binary AFH Design. The binarization of the AFH is based on the modified direct binary search method.[60] While most traditional methods use a random binary phase as their initial condition, our AFH device utilized truncated phase holography as its initial state, which enables higher convergence speed during calculation. The mean square error is computed as every pixel of the binary pattern is toggled one by one. The value of a given pixel will be preserved when the mean square error is improved, and it will be changed if the mean square error becomes worse. The iteration will stop when any change in the binary information induces a degradation of the mean square error. The binary AFH is specifically designed for high-resolution cell pattern while reducing the critical fabrication requirement for high-frequency excitation.

Flow-Field Simulation. The governing equations of acoustic streaming are eqs 22 and 23 in the Supporting Information. With the acoustic field distribution, the body force that generates acoustic streaming, which relates to acoustic particle velocity, can be calculated by eq 21 in the Supporting Information. By applying the force to the 3D simulation domain with proper boundary conditions, the governing equations are solved to yield the acoustic streaming pattern. The detailed formulation, model description, and parameters are contained in the Supporting Information.

Experimental Setup and Materials. The experimental setup includes the 3D printed box with the kinoform structures encoded

onto the bottom, a rectangular transducer (STEMiNC, U.S.A.), and a thin layer of couplant gel (Couplant D, Olympus, Japan) between them for efficient acoustic energy transmission. Three different transducers are used for generating the frequencies of 1.65/1.75 MHz (4.5 cm × 4.5 cm), 7.21 MHz (3.0 cm × 3.0 cm), and 15 MHz (1.0 cm × 1.0 cm). A function generator (AFG 3011, Tektronic, U.S.A.) generates the pulsed sinusoidal waveform with the frequencies around the center frequency of the transducer; this signal is passed through an amplifier (25A100A, Amplifier Research, U.S.A.), whose output is connected to the acoustic transducer. The height of the 3D printed container is set to be equal to the distance between the bottom structure and the image plane (e.g., 20 λ), where the fluid domain is filled with particles. The experimental phenomenon was observed under an upright microscope (BX51WI, Olympus, Japan) while the pictures and video were captured by the camera under either bright or fluorescent field. A video of 1 μm polystyrene particles was analyzed using either the PIVLab toolbox[61] in Matlab, or ImageJ (NIH, U.S.A.) to determine the flow field velocity distribution and streamlines, respectively. The acoustic field is measured using a hydrophone (HNC0100, Onda Corporation, Sunnyvale, CA) which is employed along with an oscilloscope (DPO4104, Tektronix, U.S.A.). A custom 3D scanning platform controlled by LabVIEW software (NI Corporation, TX) is used to scan the field.

For the particle/cell patterning experiment, HeLa S3 cells, NIH3T3 cells (fibroblast), and 10 μm polystyrene particles were used. Two different sizes of structures are used for patterning in large (2.5 cm × 2.5 and 2 cm × 2 cm) and small (1 cm × 1 and 0.5 cm × 0.5 cm) areas. The image plane distance determines the height of the container, and the structure size corresponds to the size of the container. The typical pulse length and repetition frequency is dependent on the designed distance between the bottom structure and the image plane. For example, with the excitation frequency of 1.65 MHz and the distance between the bottom structure and the image plane of 20 λ, the pulse length is set to be 12.1 μs (20 cycles), and the interval is 24.2 μs (40 cycles). It was also observed that with longer pulse lengths, the patterning time can be decreased but more particles will remain trapped inside the fluid domain instead of the liquid−air interface. For small-area particle patterning, 1 g L^{-1} Pluronic F68 (Sigma-Aldrich, U.S.A.) is used as the surfactant to decrease the surface tension. 5% w/v Gelatin methacryloyl (Sigma-Aldrich, U.S.A.) is used for gelating the cell pattern. Both HeLa cells and NIH3T3 cells were cultured in DMEM (Gibco, Life Technologies) containing 10% fetal bovine serum (Gibco, Life Technologies) and 1% penicillin-streptomycin (Mediatech). Cells were maintained in a cell culture incubator (Nu-4750, NuAire) with a temperature of 37 °C and a CO$_2$ level of 5%.

For particle rotation experiments, 100, 300, and 500 μm polyethylene particles (Cospheric, U.S.A.) are tested to achieve rotation in either the clockwise or counterclockwise directions. For particle/cell concentration experiments, HeLa cells, E. coli bacteria (ATCC, VA, U.S.A.), PLGA, polystyrene (Sigma-Aldrich, U.S.A.), and metal particles (nanoComposix, U.S.A.) with sizes of 1 μm, 530 nm, 400 nm, and 80 nm are all used to prove the versatility of the AFH configuration. In the particle separation experiment, 10 μm, 4.19 μm, 3 μm, 1 μm, 970 nm, and 530 nm polystyrene particles (Sigma-Aldrich, U.S.A., Bangs Laboratories, U.S.A.) with different fluorescence tags are tested in pairs, demonstrating the capacity to separate particles ranging from several micrometers to nanometers.

Cell Staining and Viability Test. For the HeLa S3 cells (ATCC, U.S.A.) staining, 1 mL of calcein AM (0.5 mmol L^{-1}, Life Technologies, U.S.A.) was added to 1 mL of cells suspended in phosphate buffer saline (PBS), followed by incubation at room temperature for 30 min. Stained cells were then centrifuged and resuspended in 1 mL of PBS. The E. coli bacteria (ATCC, U.S.A.) is stained using a BacLight Live/Dead viability kit (Thermo Fisher, U.S.A.). Fifty microliters of HeLa S3 cells is collected after AFH treatment. The cells are double-stained with calcein AM (CAM) and propidium iodide (PI) after the 20 min incubation. The viability is measured by counting CAM-positive and PI-negative cells under a microscope. For the confocal images of the cultured NIH3T3 cells,

Alexa Fluor 488 (Thermo Fisher, U.S.A.) is used for the cells, and 7-aminoactinomycin D (Thermo Fisher, U.S.A.) is used for the cell nucleus.

ASSOCIATED CONTENT

Ⓢ Supporting Information

. The Supporting Information is available free of charge at https://pubs.acs.org/doi/10.1021/acsnano.0c03754.

Comparison of simulated acoustic pressure distribution between PML boundary condition and 3D printed plastic boundary condition (Figure S1); acoustic field and interface deformation characterization (Figure S2); comparison of interface deformation before and after engineering (Figure S3); acoustic pressure and force characterization (Figure S4); typical hydrodynamic force and flow velocity (Figure S5); cell pattern feature characterization (Figure S6); particle pattern performance under different condition (Figure S7); the function of the interface deformation (Figure S8); cell pattern and culture in Petri dish (Figures S9 and 10); particle rotation characterization (Figure S11); vortex flow field characterization (Figure S12); different particle concentration demonstration (Figures S13 and 14); cell viability test (Figure S15); particle separation (Figure S16); flowchart of AFH design (Figure S17) (PDF)

Movie of patterning mechanism with simulated wave propagation (MOV)

Movie of 10 μm polystyrene particle patterning via acoustofluidic holography (MOV)

Movie of single particle rotation via acoustofluidic holography. The particle can rotate in the clockwise or counter-clockwise direction with different streaming vortex direction designs (MOV)

Movie of switching the direction of particle rotation by changing the driving frequency of the acoustofluidic holography device (MOV)

Movie of wave propagation of the acoustic vortex via acoustofluidic holography (MOV)

Movie of concentration of 10 μm polystyrene particles (blue particles in bright field) and 530 nm polystyrene particles (green fluorescent particles) (MOV)

Movie of size-based particle separation via acoustofluidic holography (MOV)

AUTHOR INFORMATION

Corresponding Author

Tony Jun Huang − *Department of Mechanical Engineering and Material Science, Duke University, Durham, North Carolina 27707, United States;* ⦿ orcid.org/0000-0003-1205-3313; Email: tony.huang@duke.edu

Authors

Yuyang Gu − *Department of Mechanical Engineering and Material Science, Duke University, Durham, North Carolina 27707, United States*

Chuyi Chen − *Department of Mechanical Engineering and Material Science, Duke University, Durham, North Carolina 27707, United States*

Joseph Rufo − *Department of Mechanical Engineering and Material Science, Duke University, Durham, North Carolina 27707, United States*

Chen Shen − *Department of Electrical and Computer Engineering, Duke University, Durham, North Carolina 27708, United States;* ⊙ orcid.org/0000-0003-3535-8494

Zeyu Wang − *Department of Mechanical Engineering and Material Science, Duke University, Durham, North Carolina 27707, United States*

Po-Hsun Huang − *Department of Mechanical Engineering and Material Science, Duke University, Durham, North Carolina 27707, United States*

Hai Fu − *Department of Mechanical Engineering and Material Science, Duke University, Durham, North Carolina 27707, United States*

Peiran Zhang − *Department of Mechanical Engineering and Material Science, Duke University, Durham, North Carolina 27707, United States;* ⊙ orcid.org/0000-0002-3873-9949

Steven A Cummer − *Department of Electrical and Computer Engineering, Duke University, Durham, North Carolina 27708, United States*

Zhenhua Tian − *Department of Aerospace Engineering, Mississippi State University, Mississippi State, Mississippi 39762, United States;* ⊙ orcid.org/0000-0002-1903-5604

Complete contact information is available at:
https://pubs.acs.org/10.1021/acsnano.0c03754

Notes

ACKNOWLEDGMENTS

REFERENCES

(1) Dobson, C. M. Protein Folding and Misfolding. *Nature* **2003**, *426*, 884−890.

(2) Svoboda, K.; Mitra, P.; Block, S. Fluctuation Analysis of Motor Protein Movement and Single Enzyme Kinetics. *Proc. Natl. Acad. Sci. U. S. A.* **1994**, *91*, 11782−11786.

(3) Grier, D. G. A Revolution in Optical Manipulation. *Nature* **2003**, *424*, 810−816.

(4) Lipfert, J.; Wiggin, M.; Kerssemakers, J. W. J.; Pedaci, F.; Dekker, N. H. Freely Orbiting Magnetic Tweezers to Directly Monitor Changes in the Twist of Nucleic Acids. *Nat. Commun.* **2011**, *2*, 11782−11786.

(5) Wang, K.; Schonbrun, E.; Steinvurzel, P.; Crozier, K. B. Trapping and Rotating Nanoparticles Using a Plasmonic Nano-Tweezer with an Integrated Heat Sink. *Nat. Commun.* **2011**, *2*, 469.

(6) Chiou, P. Y.; Ohta, A. T.; Wu, M. C. Massively Parallel Manipulation of Single Cells and Microparticles Using Optical Images. *Nature* **2005**, *436*, 370−372.

(7) Ashkin, A. Optical Trapping and Manipulation of Neutral Particles Using Lasers. *Opt. Photonics News* **1999**, *10*, 41.

(8) Rasmussen, M. B.; Oddershede, L. B.; Siegumfeldt, H. Optical Tweezers Cause Physiological Damage to Escherichia Coli and Listeria Bacteria. *Appl. Environ. Microbiol.* **2008**, *74*, 2441−2446.

(9) Collins, D. J.; Morahan, B.; Garcia-Bustos, J.; Doerig, C.; Plebanski, M.; Neild, A. Two-Dimensional Single-Cell Patterning with One Cell per Well Driven by Surface Acoustic Waves. *Nat. Commun.* **2015**, *6*, 8686.

(10) Guo, F.; Mao, Z.; Chen, Y.; Xie, Z.; Lata, J. P.; Li, P.; Ren, L.; Liu, J.; Yang, J.; Dao, M.; Suresh, S.; Huang, T. J. Three-Dimensional Manipulation of Single Cells Using Surface Acoustic Waves. *Proc. Natl. Acad. Sci. U. S. A.* **2016**, *113*, 1522−1527.

(11) Ozcelik, A.; Rufo, J.; Guo, F.; Gu, Y.; Li, P.; Lata, J.; Huang, T. J. Acoustic Tweezers for the Life Sciences. *Nat. Methods* **2018**, *15*, 1021−1028.

(12) Reboud, J.; Bourquin, Y.; Wilson, R.; Pall, G. S.; Jiwaji, M.; Pitt, A. R.; Graham, A.; Waters, A. P.; Cooper, J. M. Shaping Acoustic Fields as a Toolset for Microfluidic Manipulations in Diagnostic Technologies. *Proc. Natl. Acad. Sci. U. S. A.* **2012**, *109*, 15162−15167.

(13) Wu, J. R. Acoustical Tweezers. *J. Acoust. Soc. Am.* **1991**, *89*, 2140−2143.

(14) Wu, M.; Ouyang, Y.; Wang, Z.; Zhang, R.; Huang, P.-H.; Chen, C.; Li, H.; Li, P.; Quinn, D.; Dao, M.; Suresh, S.; Sadovsky, Y.; Huang, T. J. Isolation of Exosomes from Whole Blood by Integrating Acoustics and Microfluidics. *Proc. Natl. Acad. Sci. U. S. A.* **2017**, *114*, 10584−10589.

(15) Zhang, S. P.; Lata, J.; Chen, C.; Mai, J.; Guo, F.; Tian, Z.; Ren, L.; Mao, Z.; Huang, P. H.; Li, P.; Yang, S.; Huang, T. J. Digital Acoustofluidics Enables Contactless and Programmable Liquid Handling. *Nat. Commun.* **2018**, *9*, 2928.

(16) Rogers, P.; Gralinski, I.; Galtry, C.; Neild, A. Selective Particle and Cell Clustering at Air-Liquid Interfaces within Ultrasonic Microfluidic Systems. *Microfluid. Nanofluid.* **2013**, *14*, 469−477.

(17) Devendran, C.; Gralinski, I.; Neild, A. Separation of Particles Using Acoustic Streaming and Radiation Forces in an Open Microfluidic Channel. *Microfluid. Nanofluid.* **2014**, *17*, 879−890.

(18) Naseer, S. M; Manbachi, A.; Samandari, M.; Walch, P.; Gao, Y.; Zhang, Y. S.; Davoudi, F.; Wang, W.; Abrinia, K.; Cooper, J. M; Khademhosseini, A.; Shin, S. R. Surface Acoustic Waves Induced Micropatterning of Cells in Gelatin Methacryloyl (GelMA) Hydrogels. *Biofabrication* **2017**, *9*, 015020.

(19) Destgeer, G.; Sung, H. J. Recent Advances in Microfluidic Actuation and Micro-Object Manipulation *via* Surface Acoustic Waves. *Lab Chip* **2015**, *15*, 2722−2738.

(20) Bourquin, Y.; Reboud, J.; Wilson, R.; Cooper, J. M. Tuneable Surface Acoustic Waves for Fluid and Particle Manipulations on Disposable Chips. *Lab Chip* **2010**, *10*, 1898.

(21) Glynne-Jones, P.; Boltryk, R. J.; Hill, M. Acoustofluidics 9: Modelling and Applications of Planar Resonant Devices for Acoustic Particle Manipulation. *Lab Chip* **2012**, *12*, 1417.

(22) Li, P.; Huang, T. J. Applications of Acoustofluidics in Bioanalytical Chemistry. *Anal. Chem.* **2019**, *91*, 757−767.

(23) Wu, M.; Ozcelik, A.; Rufo, J.; Wang, Z.; Fang, R.; Huang, T. J. Acoustofluidic Separation of Cells and Particles. *Microsystems Nanoeng.* **2019**, *5*, 32.

(24) Tian, Z.; Yang, S.; Huang, P.-H.; Wang, Z.; Zhang, P.; Gu, Y.; Bachman, H.; Chen, C.; Wu, M.; Xie, Y.; Huang, T. J. Wave Number-Spiral Acoustic Tweezers for Dynamic and Reconfigurable Manipulation of Particles and Cells. *Sci. Adv.* **2019**, *5*, No. eaau6062.

(25) Bruus, H. Acoustofluidics 7: The Acoustic Radiation Force on Small Particles. *Lab Chip* **2012**, *12*, 1014.

(26) Armstrong, J. P. K.; Puetzer, J. L.; Serio, A.; Guex, A. G.; Kapnisi, M.; Breant, A.; Zong, Y.; Assal, V.; Skaalure, S. C.; King, O.; Murty, T.; Meinert, C.; Franklin, A. C.; Bassindale, P. G.; Nichols, M. K.; Terracciano, C. M.; Hutmacher, D. W.; Drinkwater, B. W.; Klein, T. J.; Perriman, A. W.; Stevens, M. M. Engineering Anisotropic Muscle Tissue Using Acoustic Cell Patterning. *Adv. Mater.* **2018**, *30*, 1802649.

(27) Kang, B.; Shin, J.; Park, H.-J.; Rhyou, C.; Kang, D.; Lee, S.-J.; Yoon, Y.; Cho, S.-W.; Lee, H. High-Resolution Acoustophoretic 3D Cell Patterning to Construct Functional Collateral Cylindroids for Ischemia Therapy. *Nat. Commun.* **2018**, *9*, 5402.

(28) Lenshof, A.; Magnusson, C.; Laurell, T. Acoustofluidics 8: Applications of Acoustophoresis in Continuous Flow Microsystems. *Lab Chip* **2012**, *12*, 1210.

(29) Schmid, L.; Weitz, D. A.; Franke, T. Sorting Drops and Cells with Acoustics: Acoustic Microfluidic Fluorescence-Activated Cell Sorter. *Lab Chip* **2014**, *14*, 3710−3718.

(30) Lee, J.; Teh, S. Y.; Lee, A.; Kim, H. H.; Lee, C.; Shung, K. K. Transverse Acoustic Trapping Using a Gaussian Focused Ultrasound. *Ultrasound Med. Biol.* **2010**, *36*, 350−355.

(31) Baresch, D.; Thomas, J.-L.; Marchiano, R. Observation of a Single-Beam Gradient Force Acoustical Trap for Elastic Particles: Acoustical Tweezers. *Phys. Rev. Lett.* **2016**, *116*, 024301.

(32) Cummer, S. A.; Christensen, J.; Alù, A. Controlling Sound with Acoustic Metamaterials. *Nat. Rev. Mater.* **2016**, *1*, 16001.

(33) Fuhrmann, D. A.; Thon, S. M.; Kim, H.; Bouwmeester, D.; Petroff, P. M.; Wixforth, A.; Krenner, H. J. Dynamic Modulation of Photonic Crystal Nanocavities Using Gigahertz Acoustic Phonons. *Nat. Photonics* **2011**, *5*, 605.

(34) Tian, Z.; Shen, C.; Li, J.; Reit, E.; Bachman, H.; Socolar, J. E. S.; Cummer, S. A.; Huang, T. J. Dispersion Tuning and Route Reconfiguration of Acoustic Waves in Valley Topological Phononic Crystals. *Nat. Commun.* **2020**, *11*, 1−10.

(35) Marzo, A.; Seah, S. A.; Drinkwater, B. W.; Sahoo, D. R.; Long, B.; Subramanian, S. Holographic Acoustic Elements for Manipulation of Levitated Objects. *Nat. Commun.* **2015**, *6*, 1−7.

(36) Veronesi, W. A.; Maynard, J. D. Nearfield Acoustic Holography (NAH) II. Holographic Reconstruction Algorithms and Computer Implementation. *J. Acoust. Soc. Am.* **1987**, *81*, 1307−1322.

(37) Marzo, A.; Drinkwater, B. W. Holographic Acoustic Tweezers. *Proc. Natl. Acad. Sci. U. S. A.* **2019**, *116*, 84−89.

(38) Ray, A.; Khalid, M. A.; Demčenko, A.; Daloglu, M.; Tseng, D.; Reboud, J.; Cooper, J. M.; Ozcan, A. Holographic Detection of Nanoparticles Using Acoustically Actuated Nanolenses. *Nat. Commun.* **2020**, *11*, 1−10.

(39) Melde, K.; Mark, A. G.; Qiu, T.; Fischer, P. Holograms for Acoustics. *Nature* **2016**, *537*, 518−522.

(40) Melde, K.; Choi, E.; Wu, Z.; Palagi, S.; Qiu, T.; Fischer, P. Acoustic Fabrication *via* the Assembly and Fusion of Particles. *Adv. Mater.* **2018**, *30*, 1704507.

(41) Ai, Y.; Sanders, C. K.; Marrone, B. L. Separation of Escherichia Coli Bacteria from Peripheral Blood Mononuclear Cells Using Standing Surface Acoustic Waves. *Anal. Chem.* **2013**, *85*, 9126−9134.

(42) Friend, J.; Yeo, L. Y. Microscale Acoustofluidics: Microfluidics Driven *via* Acoustics and Ultrasonics. *Rev. Mod. Phys.* **2011**, *83*, 647−704.

(43) Wiklund, M.; Green, R.; Ohlin, M. Acoustofluidics 14: Applications of Acoustic Streaming in Microfluidic Devices. *Lab Chip* **2012**, *12*, 2438.

(44) Nama, N.; Huang, P.-H.; Huang, T. J.; Costanzo, F. Investigation of Acoustic Streaming Patterns around Oscillating Sharp Edges. *Lab Chip* **2014**, *14*, 2824−2836.

(45) Ahmed, D.; Chan, C. Y.; Lin, S.-C. S.; Muddana, H. S.; Nama, N.; Benkovic, S. J.; Huang, T. J. Tunable, Pulsatile Chemical Gradient Generation *via* Acoustically Driven Oscillating Bubbles. *Lab Chip* **2013**, *13*, 328−331.

(46) Bertin, N.; Chraïbi, H.; Wunenburger, R.; Delville, J. P.; Brasselet, E. Universal Morphologies of Fluid Interfaces Deformed by the Radiation Pressure of Acoustic or Electromagnetic Waves. *Phys. Rev. Lett.* **2012**, *109*, 1−5.

(47) Gor'kov, L. On the Forces Acting on a Small Particle in an Acoustic Field in an Ideal Fluid. *Sov. Phys. Dokl* **1962**, *6*, 773.

(48) Brown, M. D.; Cox, B. T.; Treeby, B. E. Design of Multi-Frequency Acoustic Kinoforms. *Appl. Phys. Lett.* **2017**, *111*, 244101.

(49) Bourquin, Y.; Syed, A.; Reboud, J.; Ranford-Cartwright, L. C.; Barrett, M. P.; Cooper, J. M. Rare-Cell Enrichment by a Rapid, Label-Free, Ultrasonic Isopycnic Technique for Medical Diagnostics. *Angew. Chem., Int. Ed.* **2014**, *53*, 5587−5590.

(50) Brown, M. D. Phase and Amplitude Modulation with Acoustic Holograms. *Appl. Phys. Lett.* **2019**, *115*, 053701.

(51) Brown, M. D.; Allen, T. J.; Cox, B. T.; Treeby, B. E. Control of Optically Generated Ultrasound Fields Using Binary Amplitude Holograms. In *2014 IEEE International Ultrasonics Symposium*; IEEE, 2014; 1037−1040.

(52) Brown, M. D.; Jaros, J.; Cox, B. T.; Treeby, B. E. Control of Broadband Optically Generated Ultrasound Pulses Using Binary Amplitude Holograms. *J. Acoust. Soc. Am.* **2016**, *139*, 1637−1647.

(53) Mueller, R. K. Acoustic Holography. *Proc. IEEE* **1971**, *59*, 1319.

(54) Tung, K.-W.; Chung, P.-S.; Wu, C.; Man, T.; Tiwari, S.; Wu, B.; Chou, Y.-F.; Yang, F.; Chiou, P.-Y. Deep, Sub-Wavelength Acoustic Patterning of Complex and Non-Periodic Shapes on Soft Membranes Supported by Air Cavities. *Lab Chip* **2019**, *19*, 3714−3725.

(55) Mellin, S.; Nordin, G. Limits of Scalar Diffraction Theory and an Iterative Angular Spectrum Algorithm for Finite Aperture Diffractive Optical Element Design. *Opt. Express* **2001**, *8*, 705.

(56) Matsushima, K.; Shimobaba, T. Band-Limited Angular Spectrum Method for Numerical Simulation of Free-Space Propagation in Far and near Fields. *Opt. Express* **2009**, *17*, 19662−19673.

(57) Williams, E. G. *Fourier Acoustics: Sound Radiation and Nearfield Acoustical Holography*; Elsevier: London, 1999.

(58) Zeng, X.; McGough, R. J. Evaluation of the Angular Spectrum Approach for Simulations of Near-Field Pressures. *J. Acoust. Soc. Am.* **2008**, *123*, 68−76.

(59) Teo, T.; Reid, J. M. Multifrequency Holography Using Backpropagation. *Ultrason. Imaging* **1986**, *8*, 213−224.

(60) Leportier, T.; Park, M. C.; Kim, Y. S.; Kim, T. Converting Optical Scanning Holograms of Real Objects to Binary Fourier Holograms Using an Iterative Direct Binary Search Algorithm. *Opt. Express* **2015**, *23*, 3403.

(61) Thielicke, W.; Stamhuis, E. PIVlab-towards User-Friendly, Affordable and Accurate Digital Particle Image Velocimetry in MATLAB. *J. Open Res. Softw.* **2014**, *2*, No. e30.